Discover Mechanical Engineering

Discover

Brief Communication

Investigating mechanosensitive channels activation in concert with the mechanical properties of red blood cells

Nicoletta Braidotti[1,2] · Catalin Dacian Ciubotaru[2] · Davide Rizzo[3] · Lorenzo Bergamo[3,4] · Annalisa Bernareggi[3] · Dan Cojoc[2]

Received: 31 August 2023 / Accepted: 17 October 2023
Published online: 23 October 2023

Abstract
The activity of the mechanosensitive Ca^{2+} permeable channels expressed in the membrane of the red blood cells (RBC) is determined both by the mechanical stimuli and the mechanical properties of the cell. Therefore, it is of most importance to correlate the triggering stimulus with the mechanical properties. In this paper, we propose an approach to determine the activation pressure of the mechanosensitive channels and concomitantly evaluate cell mechanical properties as Young's Modulus, membrane tension and viscosity, for individual cells. Cell deformation was accomplished by micropipette aspiration with a controlled pressure ramp and recorded by brightfield imaging to determine the mechanical properties. The Ca^{2+} transient was concomitantly monitored by fluorescence imaging, to get the activation pressure. The technique was validated comparing the behavior of three pools of RBCs, probed at different intervals of time after the cell suspension preparation by the same mechanical stimuli. We found relevant changes of the activation pressure, associated with the alteration of the mechanical properties, the latest becoming significant with the passage of time. Our approach opens a new direction to investigate the correlation between mechanosensitivity and mechanical properties for individual RBCs, which can be extended to other cells, in suspension or plated, under controlled environmental conditions.

1 Introduction

It is known that the main function of the Red Blood Cells (RBCs) in the human body is to oxygenate the tissues and collect back the carbon dioxide [1]. To accomplish this function, RBCs require exceptional deformability due to the geometrical and chemical constraints in the circulatory system. Moreover, this property must be maintained for about 100,000 circulation cycles during their 120 days life cycle [1, 2]. RBCs have a biconcave shape minimizing the volume to surface area (60% the volume of a sphere with the same area surface) and a flexible membrane which confer them the possibility to easily change shape. The membrane encapsulates the hemoglobin solution and the underlying membrane skeleton, a two-dimensional network composed by actin filaments interconnected by spectrin tetramers bound

Supplementary Information The online version contains supplementary material available at https://doi.org/10.1007/s44245-023-00026-3.

✉ Dan Cojoc, cojoc@iom.cnr.it; Nicoletta Braidotti, nicoletta.braidotti@phd.units.it; Catalin Dacian Ciubotaru, ciubotaru@iom.cnr.it; Davide Rizzo, davide.rizzo@studenti.units.it; Lorenzo Bergamo, lorenzo.bergamo@mr.mpg.de; Annalisa Bernareggi, abernareggi@units.it | [1]Department of Physics, University of Trieste, Via A. Valerio 2, 34127 Trieste, Italy. [2]Materials Foundry Institute, National Research Council of Italy (CNR), Area Science Park-Basovizza, Strada Statale 14, Km 163,5, 34149 Trieste, Italy. [3]Department of Life Sciences, University of Trieste, Via Fleming 22, 34127 Trieste, Italy. [4]Present Address: Max Planck Institute for Medical Research, Jahnstraße 29, 69120 Heidelberg, Germany.

to transmembrane proteins [3, 4]. This structure grants to RBC an exceptional deformability, as well as the resistance to bending and shear stress [5]. However, these distinctive mechanical properties can drastically undergo changes under some pathological conditions, as for example in sickle cell disease, malaria, diabetes mellitus, and sepsis [6, 7]. Therefore, determining the mechanical properties of RBCs under different conditions had acquired a lot of interest and different techniques have been developed in the last two decades to this purpose: micropipette aspiration [8, 9], microfluidics [10], atomic force microscopy [11], ektacytometry [12], optical tweezers [13], optical stretcher [14] and acoustic tweezers [15]. All these techniques allow the measurement of single cells deformation under a controlled mechanical stress by using optical microscopy imaging and force recording, followed by the application of different biomechanical models to extract mechanical parameters as Young's Modulus, bending modulus, membrane tension or viscosity. Beside these mechanical properties, morphological properties such as cell volume or surface area are also considered to assess cell functionality [16, 17]. For instance, volume regulation was evaluated in pathologies resulting from either overhydration and dehydration of erythrocytes [18].

The exchange of Ca^{2+}, Na^{+} and K^{+} cations through the membrane ion channels plays an important role for the regulation of the RBC volume [2, 19]. Recently, Piezo1 channel was demonstrated to contribute in volume regulation [2] and gene mutations had been linked with RBC dehydration and related pathologies [20].

Piezo1 is a mechanosensitive permeable cation channel discovered by Coste and collaborators [21] which can be activated by changes in the membrane tension [22–25], regulating in turn the influx of Ca^{2+} in RBC in response to the membrane stretch [2].

The influx of Ca^{2+} through the Piezo1 channel was shown to trigger the Gárdos channel and release of K^{+} ions and water from the cell [26], regulating in this way the RBC volume [2]. Recently, the presence of the transient receptor potential channel vanilloid type 2 (TRPV2) was also reported in RBCs [27]. TRPV2 is a mechanosensitive non-selective Ca^{2+} permeable cation channel which contributes to the osmotic balance [27] and Ca^{2+} dissipation in storage lesion [28]. Even if TRP channels family is known to take part into the mechanosensory cell system, most of them have been demonstrated to be insensitive to membrane stretch [29] and being activated downstream of other channels such as Piezo1 [30–32].

The activation of the mechanosensitive channels depends on both the external mechanical stimuli and the mechanical properties of the cell. However, channel gating and mechanical properties of cells are usually studied separately on different pools of cells, and, sometimes, even employing different experimental approaches [11, 33]. Therefore, the possibility to make a correlation between gating behavior and mechanical properties for individual cells is lost in this way. Recently, we have introduced a bimodal imaging approach enclosing fluorescence and brightfield imaging to monitor calcium transients and stimulus probe position on the cell and study the activation of mechanosensitive channels in neuronal cells by piconewton forces applied by optical tweezers [34, 35]. Moreover, a micropipette aspiration technique with concurrent RBC morphology imaging and intracellular calcium has also been reported by another group for the determination of the RBC calcium dynamic range [36, 37]. Here we implement a similar bimodal imaging in combination with the micropipette aspiration technique, however our approach is characterized by the multiple complementary information achievable at the same time from single cells. In fact, we determined the activation pressure by fluorescence Ca^{2+} imaging and simultaneously evaluated the mechanical properties (Young's Modulus, membrane tension, viscosity) by monitoring cell deformation versus the aspiration pressure. To validate the technique, we investigated human RBCs at three distinct intervals of time: 0–20, 20–40 and 40–60 min after their preparation, showing that both the activation pressure and the mechanical properties were subjected to changes.

2 Materials and methods

2.1 Combined micropipette aspiration and bimodal imaging setup

The experimental setup is based on our previously developed systems combining optical tweezers for mechanical stimulation with piconewton forces, electrophysiology, and bimodal imaging [34, 35]. Here, the employed micropipette aspiration module allows us to apply negative pressures in the range 0 to − 60 mbar, attracting single RBC to the pipette tip and drawing them into a capillary.

The picture in Fig. 1a illustrates the setup with the inverted microscope (Olympus IX 81), the pressure control (Press-ctrl) Flow ZE (Fluigent, Le Kremlin-Bicêtre, France), the dual CCD camera Orca D2 (Hamamatsu, Tokyo, Japan), the micromanipulator MM (Narishige, Tokyo, Japan), the halogen lamp (HL), the LED system (X-Cite XLED1, Excelitas Technology, Waltham, MA, USA), the sample chamber and the motorized microscope stage (SC-MS).

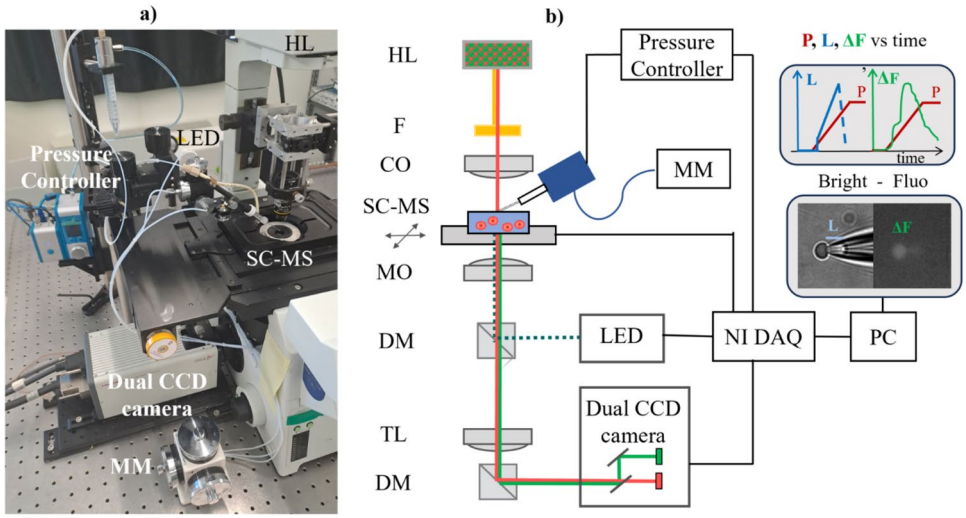

Fig. 1 Combined micropipette aspiration and bimodal imaging setup. **a** picture of the setup; **b** scheme of the setup: *HL* halogen lamp, *F* optical filter, *CO* condenser objective, *SC-MS* sample chamber and microscope stage, MO- microscope objective, *DM* Dichroic mirrors, *TL* tube lens, *MM* micromanipulator; the bimodal imaging (inset) shows the cell entering the micropipette and forming a tether of length L (left side) together with the fluorescence corresponding to the activation of the mechanosensitive channels (right); the top inset shows the variation of the applied pressure P, tether length L and fluorescence ΔF

As it is shown in the layout of the setup (Fig. 1b), the cells are placed in a fluidic chamber (Coverslip clamp chamber. ALA Sci. Instr., Farmingdale, NY, USA) and illuminated by the HL through a high pass optical filter F to remove the light with wavelength $\lambda > 750$ nm. Thus, brightfield imaging is achieved, without exciting the fluorescence dye, through a microscope objective MO (Olympus 60X, NA 1.25, Olympus Corporation, Tokyo, Japan) on one of the two CCD sensors of a dual CCD camera (Orca D2, Hamamatsu, Tokyo, Japan). A LED at $\lambda = 460$ nm (X-Cite XLED1, Excelitas Technology, Waltham, MA, USA) is used to excite the calcium indicator Fluo-4 (F10471, Fluo-4 Direct™ Calcium Assay Kit, Invitrogen, Waltham, MA, USA) and the fluorescence image is obtained on the second sensor of the dual camera.

Applying a low negative pressure ramp (typically -2 mbar/s) the cells move towards the micropipette until the closest one touches the tip and starts to deform expressing a tether of which length L increases with the increasing pressure P (inset Fig. 1b). At higher pressure the cell is then eventually sucked into the pipette, in the region with larger diameter. The signals from the pressure control, LED system and camera are acquired by a digital acquisition board NI DAQ (National Instruments, Austin, TX, USA) and controlled by custom software, allowing the synchronization of the pressure, cell deformation—tether elongation, and fluorescence signals. Each recording was performed using the LED at 30% of max power with 50 ms exposure, to minimize the bleaching of the fluorescence dye, and at an acquisition rate of 7 frames per second to properly follow the cell deformation. The differential fluorescence signal for the actual frame, *s* is calculated as: $\Delta Fs = (Fs-F0)/F0$, where *Fs* is the mean fluorescence intensity over a circular region of interest (ROI) of which diameter is defined by the cell in contact with the pipette, and *F0* is the mean intensity for the first 4 frames, calculated over the same ROI. The background signal ΔFb is measured in the same manner for a background ROI. The final fluorescence signal is calculated as: $\Delta F = \Delta Fs - \Delta Fb$. In few cases we observed cell rupture after consistent pressure values, where the fluorescence suddenly peaks to high levels (see Supplementary Material, Supplementary Movie 1). These cases were excluded from the statistic.

2.2 Definition of the activation pressure and mechanical parameters

By plotting the pressure and fluorescence signals versus time, as in the example shown in Fig. 2a, we determined relevant pressure values as defined below:

- **Contact pressure, *Pc*** is the pressure corresponding to the first elevation of the fluorescence signal; this small signal is due to the change of the cell shape when it gets in contact with the pipette;
- **Activation pressure, *Pa*** is the pressure corresponding to the second fast elevation of the fluorescence signal, reflecting the Ca^{2+} gating as a consequence of mechanosensitive channels opening; *Pa* is chosen as the pressure

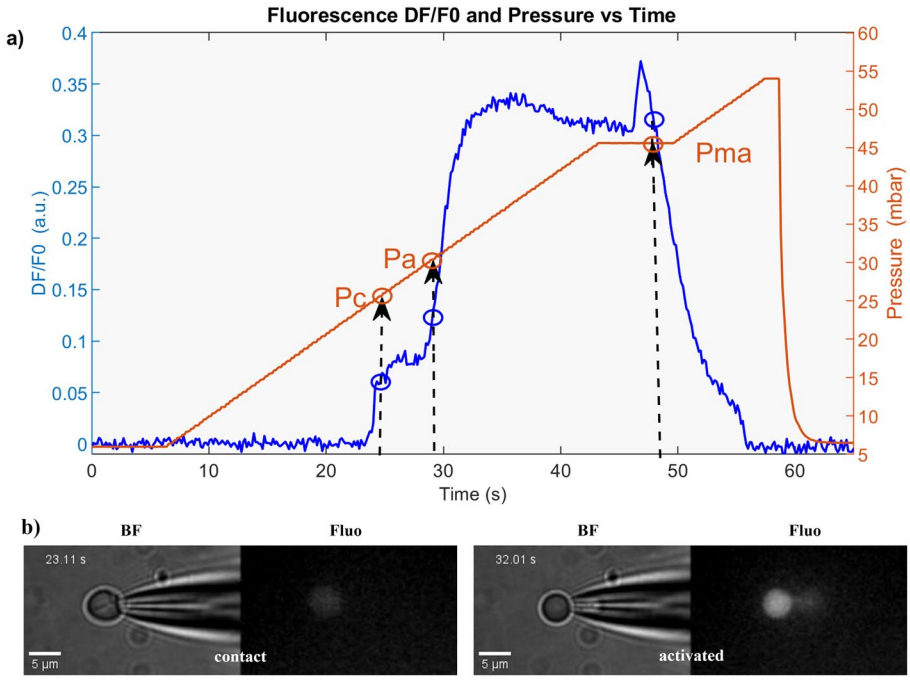

Fig. 2 Example of data plot from a typical aspiration experiment. **a** The pressure values: *Pc, Pa* and *Pma* are determined using the differential fluorescence ΔF curve and the criteria defined in Sect. 2.2. The scale relative to the aspiration (negative) pressure is reported in absolute values. **b** Two bimodal images showing the cell morphology and the fluorescence intensity at two different instants of the aspiration: the cell gets in contact (left) and the tether is pulled into micropipette (right) inducing the mechanosensitive channels activation indicated by the elevated fluorescence intensity

value corresponding to the differential fluorescence value $\Delta F = \Delta Fc + c^{*}\Delta Fm$, where ΔFc and ΔFm are the fluorescence values at contact and the maximum fluorescence value and c is a constant chosen by the user (we chose $c = 0.1$ here).

- **Maximum aspiration pressure, *Pma*** is the pressure taken at the time when the fluorescence signal ΔF drops down: $\Delta Fma = 0.9^{*}\Delta Fm$, indicating the detachment of the cell from the tip of the pipette. This event is confirmed also by the cell morphology change observed in brightfield.

The plot of the pressure versus the tether length (L) allows to determine the elongation $\Delta L = L\text{-}L0$, with respect to the value at the contact ($L0$). The variation of the cell diameter during aspiration can also be determined from the brightfield movie.

With the above explained pressure, fluorescence and morphological parameters we can introduce some other characterizing the viscoelastic properties of the cell, using the definitions introduced by Hochmuth [38].

1) Young's modulus, E, given in [Pa]:

$$E = 11.4 * \frac{\Delta P}{\Delta L} * Dp \tag{1}$$

where: $\Delta P = Pma\text{-}Pc$, $\Delta L = L\text{-}L0$, Dp is the pipette diameter

2) Cortical tension, Tc, in [N/m]:

$$Tc = 1.1 * E * Dp \tag{2}$$

3) Velocity of the tether pulling into pipette, Vt, in [µm/s]:

$$\Delta L = Lma - L0, Vt = \frac{\Delta L}{\Delta t} \tag{3}$$

where ΔL, is the elongation of the membrane tether between the initial length L0 evaluated just after the contact to the maximum length Lma reached just before the cell is sucked into the larger diameter part of the capillary.

4) Cell Viscosity, v in [Pa s]:

$$v = \frac{Dp\Delta P}{12\left(\frac{\Delta L}{\Delta t}\right)\left(1 - \frac{Dp}{Dc}\right)} \tag{4}$$

where *Dc* is the diameter of the cell outside the tip.

2.3 Pipettes preparation

Pipettes were obtained from borosilicate capillaries (Warner Instruments, Hamden, CT, USA, model No. G150-6, OD: 1.50 mm, ID: 0.86 mm, length: 15 cm) using the Narishige puller PP-830 (Narishige, Tokyo, Japan). Temperature steps were selected to obtain pipette with a diameter of about 2 µm. To refine the tips, the polishing was achieved with the Narishige micro-forge MF-830 (Tokyo, Japan). The inner diameter (2 µm) is maintained for a length of 12 µm. After that point the diameter increases abruptly to the original diameter (0.86 mm), as shown in Fig. 2b, allowing the collection of many cells and hence multiple experiments with the same pipette.

2.4 Cell culture and sample preparation

Human blood samples from adult patients were anonymously provided by "Maggiore" Hospital, Trieste, stored at + 4 °C and used within the following 3 days. RBCs were obtained from centrifugations and dilution steps in DPBS (14190–094, Thermo Fisher Scientific, Waltham, MA, USA). Then the cell suspension was incubated in 1 × Fluo4 solution (F10471, Fluo-4 Direct™ Calcium Assay Kit, Invitrogen, Waltham, MA, USA) for one hour in the dark at + 37 °C. Cells were then washed by centrifugations in DPBS three times and one more wash was performed in HBSS (L0612, Biowest, Nuaillé, France). Thereafter, cells were 1:100 diluted in a 1:1 solution of HBSS and RPMI (61870010, RPMI 1640 Medium, GlutaMAX™ Supplement, Thermo Fisher Scientific, Waltham, MA, USA) with 10% of Fetal Bovin Serum (FBS). Cells were let to sit in the dark for 20 min. Finally, the final sample was obtained by diluting 1:100 once more the cellular suspension and stored at room temperature. We run experiments on 10 different patients. Each sample was subjected to a maximum acquisition time of 1 h. Post-experiments and during data analysis, investigated cells were then grouped into three pools (P1, P2 and P3) relative to three different intervals of time (0–20, 20–40, 40–60 min) respect to the time passed from the sample preparation.

3 Results and discussions

To validate our approach, we explored for a possible correlation between the aspiration pressure required to activate/open the mechanosensitive channels and the mechanical properties of human RBCs. During the preliminary experiments, intended to optimize the aspiration protocol, the sample with RBCs was kept about 1 h in the sample chamber to perform different aspiration experiments. Since from the brightfield images we noticed the RBCs tendency to deform slightly differently after 20–30 min we decided to run a deeper analysis. Therefore, we considered three pools of cells, according to the time passed from cell preparation: P1, 0–20 min; P2, 20–40 min; P3, 40–60 min. The same experimental protocol, described in Sect. 2.1, was applied to each of the three groups of cells.

An example of a typical experiment is illustrated in Fig. 2, showing the pressure and the fluorescence signals as a function of time (Fig. 2a), and two bimodal images showing the cell deformation and the Ca^{2+} mobilization at two different moments (Fig. 2b). The time lapse for the cell deformation and Ca^{2+} gating can be observed in Supplementary Movie 2.

We ran experiments with human RBCs from 10 different patients in 6 different days, samples were prepared by following the protocol described in Sect. 2.4. We tested N1 = 130 cells for the first pool P1, N2 = 70 cells for the second pool P2 and N3 = 50 cells for the third pool P3 of RBCs. The differential fluorescence ΔF was firstly evaluated to determine the activation values ΔFa corresponding to the channel activation. Responding cells were considered if $\Delta Fa > 0.02$, a value which is about 4 times higher than the maximum of the fluorescence noise, extracted from the background fluorescence fluctuations during the experiment. Thus, excluding cells which did not satisfy the responding criterium, the number of considered cells for further analysis was reduced to: N1 = 108, N2 = 42 and N3 = 21 respectively. This means that about 83.1% from the first pool, 60% from the second pool and 42% from the third pool of cells responded to the mechanical stimuli, indicating that the activation probability is reduced during the storing time. We assigned this trend to possible changes of the cell properties but also to the fluorophore instability and bleaching.

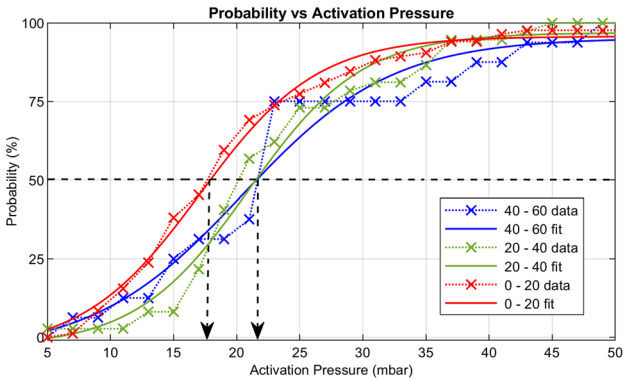

Fig. 3 Activation Pressure distributions, experimental data (dotted line) fitted with the Boltzmann fit function for the three pools of cells: P1 (red), P2 (green), P3 (blue)

Table 1 Mean and standard deviation values of the activation pressure and four mechanical parameters of the RBCs tested by micropipette aspiration

	P1 0–20 min		P2 20–40 min		P3 40–60 min	
	Mean	std	Mean	std	Mean	std
Activation pressure, *Pa* [mbar]	22.55	11.3	24.76	8.8	25.47	11.5
Young's modulus, *E* [Pa]	57.83	46.3	67.24	49.8	113.57	48.4
Membrane tension, *Tc* [pN/um]	96.7	76.1	125.1	87.5	187.4	79.8
Tether velocity, *Vt* [um/s]	1.13	1	1.12	0.9	0.54	0.5
Viscosity, *v* [Pa s]	208	204	277	244	527.02	331.5

The activation pressures values and their distributions were calculated for the responding cells and data were fitted with the Boltzmann function [39]:

$$Prob = \frac{1}{1 + e^{\frac{-(P-b)}{a}}} + c \tag{5}$$

where *Prob* is the activation probability corresponding to pressure *P*, and a, *b* and *c* are numerical parameters defining the shift and tilt of the fitting curve. When $P = b$, the probability $Prob = 50\%$ and the corresponding pressure value, *P50* is considered as the activation pressure characterizing the pool of cells. The experimental data and the fitted curves are presented in Fig. 3 for the three groups of cells. The activation pressures corresponding to 50% probability (P50) and relative to the fitting parameter b, are: $P50\_1 = 18.6$ mbar, $P50\_2 = P50\_3 = 21.65$ mbar, showing that the activation pressure value P50 for the first pool of cells (0–20 min) is lower by about 3 mbar than the activation pressure corresponding to the second (20–40 min) and third (40–60 min) pools. These values fall in the range of pressures previously investigated [2, 36] and observed to be necessary for calcium mobilization in RBCs. In particular, due to the absence of intracellular stores, the signal observed should be assigned to Ca^{2+} influx which is dependent on Piezo1 activation as suggested by Cahalan and collaborators [2]. The values of the second fitting parameter, *a* indicating the spreading of the data, are: $a\_1 = 4.6$, $a\_2 = 4.8$, $a\_3 = 5.9$. The values of the parameter c, are close to 0 for all the three fits (– 0.04, – 0.06, – 0.05). As one can notice from the Fig. 3, the first two curves, corresponding to pools P1 (red) and P2 (green) are similar, while the third (P3—blue) is tilted more, indicating a larger spreading of the activation pressure data.

By calculating the mean and standard deviation of the activation pressure (Pa) values for each of the three pools of cells (Table 1), we observed that the mean values are higher than the activation pressures at 50% probability (P50) in all three cases. The standard deviations are big, indicating wide data spreading. Moreover, since the distributions are not normal (see Fig. 4a, b) and the samples are independent and of different sizes, we compared them by using the Wilcoxon rank sum test, which takes the null hypothesis as equal medians [40]. The box plots illustrated in Fig. 4c indicate that the null hypothesis is rejected (p-value, $p < 0.05$) only for the pair of samples P1-P2 ($p = 0.01$), which means that the activation pressure medians of the pools P1 and P2 are significantly different. Few experiments (cells) for which the activation pressure was found out of the range [5–60 Pa] were excluded from the box plots in Fig. 4c, even if they satisfied the criterium of the fluorescence threshold, because too low or too high values for the activation pressure are not practical.

In conclusion, we found that the activation pressure at 50% probability, P50 calculated by fitting the experimental data with the Bell's function was lower for P1 than P2 and P3. Moreover, the activation pressure mean values indicated

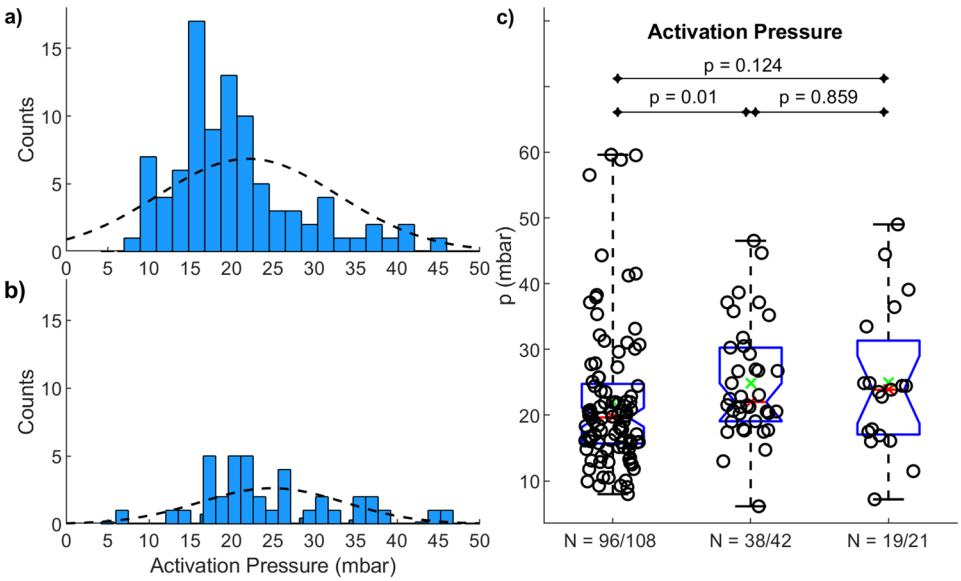

Fig. 4 Histograms of the activation pressure distributions for the pools of cells P1, 0–20 min (**a**), P2, 20–40 min (**b**) and the box plot representation with the p-value resulting from the Wilcoxon test for all the three pools of cells (**c**). N represents the number of cells for which the values of the activation pressure are within a practical range: *Pa* [5–60 mbar]

an increase from P1, to P2 and P3 with a significant difference between P1 and P2. Altogether these results suggest that storage in the sample chamber alters RBC mechanosensitivity even after just 20 min.

Since the cortical membrane tension was recognized as one of the cell mechanical parameters which can modulate the activity of the mechanosensitive channels [22] and based on the possibility to run concurrent measurement of the cell deformation in our approach, we decided to determine also the associated mechanical parameters: Young's Modulus (E), membrane cortical tension (*Tc*), the flow velocity (*Vt*) of the cell tether pulled into the pipette and the viscosity (*v*), as defined in Sect. 2.2.

The mean and standard deviation values shown in Table 1 indicate that the storing time produces an increment in the values of the following parameters: *E, Tc* and *v,* while *Vt* decreases. However, by checking the distributions we found that they are once again not normal and hence, to interpret the data, we proceeded with the box plot representation and the Wilcoxon test.

The results are shown in Fig. 5 and indicate a significant difference for both pools P1 and P2 with respect to pool P3, while the differences between P1 and P2 are not significant.

In the comparation of these results with the activation pressure ones, one can observe that the mechanical properties are also altered with the storing time, but this alteration is retarded with respect to the activation pressure change. Interestingly, the activation pressures at 50% probability for P2 and P3 are equal, and higher than the activation pressure for P1, suggesting that after a relatively fast change, this parameter remains stable. This is also confirmed by the significant difference found in the activation pressure mean values by comparing P1 and P2. Nonetheless, we also obtained two unexpected results: (1) cells mechanical properties are changed after about 40 min, and (2) the alteration of the activation pressure preceded that of the mechanical properties.

It is known that RBC mechanical properties can deteriorate during anaerobic storage, but this was observed after days and not after just tens of minutes [41]. The alteration after about 40 min that we observed here might be due to the experimental conditions, which are different from the blood storage conditions. In fact, for our Ca^{2+} imaging in aspiration experiments, cells are loaded with Fluo-4 fluorescence dye and maintained at low concentration in buffer solution consisting of HBSS, RPMI and FBS. Despite differences in interval times, our results are consistent with literature. For example, the increment in cell stiffness, as evidenced by the increment in Young's Modulus assessed by us, agrees with storing time experiments performed by Xu and collaborators [42]. Moreover, the increment in viscosity which accompanies the stiffening is also well demonstrated [43–45]. At the same time also the rise in tension is compatible with published observations [46], while the reduction in cell velocity which suggests an increased resistance to flow as a consequence of increased viscosity finds also support in literature [3, 47].

Our work evidenced a relatively short experimental shelf time (about 1 h), after which the morphology and the deformation properties of the cells changed considerably, making the experiments irrelevant. Thus, the time becomes a critical methodological aspect to be considered when this type of cell mechanics experiment is planned for RBCs and possibly also for other types of cells.

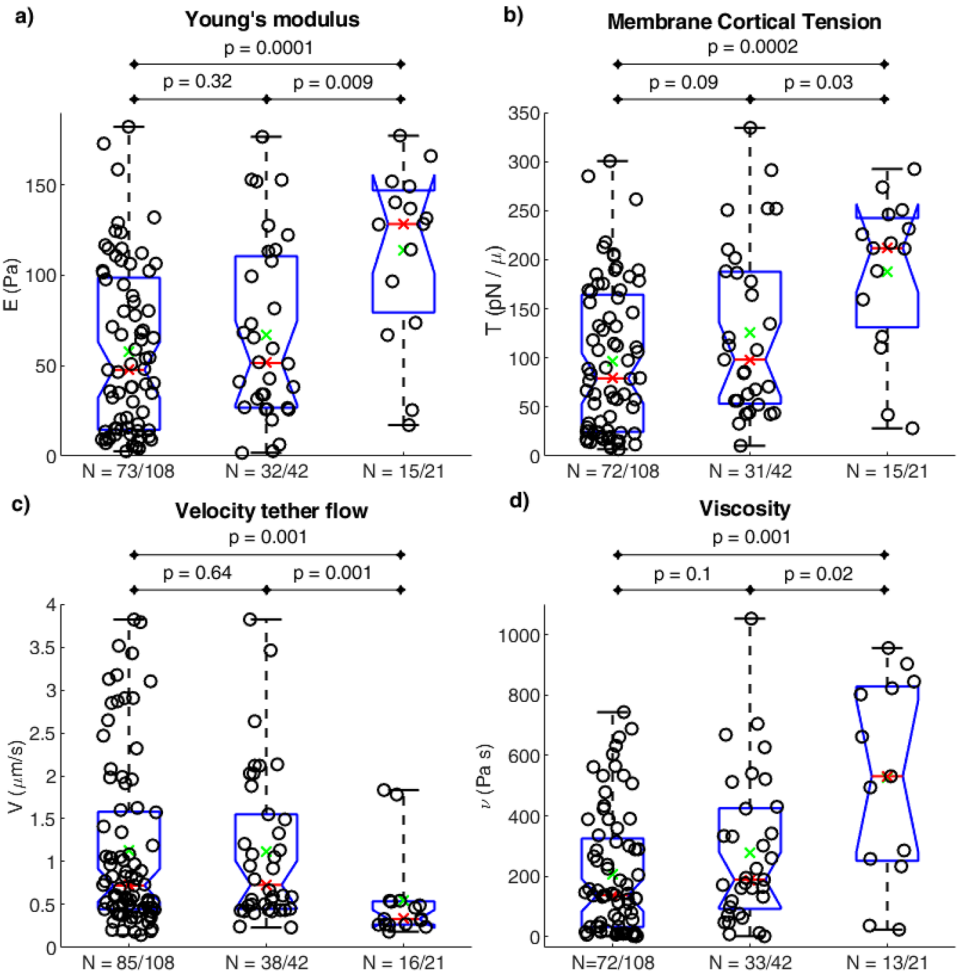

Fig. 5 Box plot and Wilcoxon test (p-values) for the mechanical parameters: Young's Modulus (**a**), cortical membrane tension (**b**), tether flow velocity (**c**) and viscosity (**d**). N represents the number of cells [over the number of responding cells)] for which the values of the mechanical parameter are within a practical range: *E* [5–185 Pa], *Tc* [5–350 pN/μm], *Vt* [0.1–4 μm/s], *v* [5–1100 Pa s]

As for the second unexpected result, although we have not yet found a convincing explanation for the preceding of channel gating variations to the mechanical properties changes, we hypothesize that the local membrane-associated elements such as cholesterol may result firstly affected inducing membrane tension alterations [48] and mechanosensitive channels activity modulation [49]. This may be then followed by cytoskeletal reorganization which effect emerges at longer time scale (> 40 min) and mechanical properties impairment. It's reasonable to think that the activation pressure might result further affected after a significant alteration of the mechanical properties. Unfortunately, we could not follow properties variation for more than 1 h with the cells in the sample chamber due to the instability of the fluorophore.

4 Conclusions

We introduced a new approach for measuring the activation pressure of mechanosensitive channels in RBCs, at the same time with some mechanical properties evaluation. A bimodal microscopy including brightfield and epifluorescence imaging was implemented to monitor in parallel cell deformation and mechanosensitive channels activation during RBCs aspiration into a glass micropipette by a negative pressure which decreases at a constant rate. Even if a similar approach has no previous reports from our knowledge, we compared our results to published data obtained by independent investigations with different techniques. The analogy found in our results with respect to the literature reported ones is the proof that our bimodal approach can precisely measure both mechanical properties and assess channel functionality at the same time with superior strengths.

We found that both activation pressure and the mechanical properties change during 1 h cells storing in the sample chamber. Unexpectedly, we found that the activation pressure was altered before mechanical parameters changes could be noticed and remained stable after these changes occurred. We think that the alteration of the mechanical properties

after longer times would further influence the activation pressure but, unfortunately, we could not run experiments longer than 1 h to check this hypothesis, due to the fluorophore instability. To further understand how much the activation pressure is correlated to altered mechanical properties of the cell, in future we plan to use drug treatment to induce significant changes in the actin filaments of the cytoskeleton, and thus induce mechanical properties changes in shorter time.

Acknowledgments We acknowledge Dr. Francesca Siriani, the head of the Laboratorio Analisi Unico from the Azienda Sanitaria Universitaria Giuliana Isontina (ASUGI) for the kind support for blood samples.

Author contributions DC, CDC and NB contributed to the study conception and design. AB revised critically the work. Material preparation, data collection and analysis were performed by NB, DR, LB. The first draft of the manuscript was written by DC and NB and all authors commented on previous versions of the manuscript. All authors read and approved the final manuscript.

Funding No funding was received for conducting this study.

Data availability The complete data can be made available upon request.

Code availability Not applicable.

Declarations

Ethics approval and consent to participate Ethical review and approval were waived for this study due to the hospital department leaving off the clinical samples, after completing the necessary clinical analyses and removing sensitive patient data.

Competing interests The authors declare no competing interests.

References

1. Besedina NA, et al. Persistent red blood cells retain their ability to move in microcapillaries under high levels of oxidative stress. Commun Biol. 2022;5(1):659.
2. Cahalan SM, et al. Piezo1 links mechanical forces to red blood cell volume. eLife. 2015;4:e07370.
3. Gokhin DS, et al. Dynamic actin filaments control the mechanical behavior of the human red blood cell membrane. Mol Biol Cell. 2015;26(9):1699–710.
4. Vaisey G, et al. Piezo1 as a force-through-membrane sensor in red blood cells. eLife. 2022;11:e82621.
5. Li X, et al. 2014 Probing red blood cell mechanics, rheology and dynamics with a two-component multi-scale model. Philos Trans. 2021;372:20130389.
6. Peng Z, et al. Lipid bilayer and cytoskeletal interactions in a red blood cell. Proc Natl Acad Sci. 2013;110(33):13356–61.
7. Ebrahimi S, Bagchi P. A computational study of red blood cell deformability effect on hemodynamic alteration in capillary vessel networks. Sci Rep. 2022;12(1):4304.
8. Evans EA. Bending elastic modulus of red blood cell membrane derived from buckling instability in micropipet aspiration tests. Biophys J. 1983;43(1):27–30.
9. Wang H, et al. Micropipette-based biomechanical nanotools on living cells. Eur Biophys J. 2022;51(2):119–33.
10. Wei Q, et al. Evolution of surface area and membrane shear modulus of matured human red blood cells during mechanical fatigue. Sci Rep. 2023;13(1):8563.
11. Barns S, et al. Investigation of red blood cell mechanical properties using AFM indentation and coarse-grained particle method. Biomed Eng Online. 2017;16(1):140.
12. Renoux C, et al. Impact of surface-area-to-volume ratio, internal viscosity and membrane viscoelasticity on red blood cell deformability measured in isotonic condition. Sci Rep. 2019;9(1):6771.
13. Avsievich T, et al. The advancement of blood cell research by optical tweezers. Rev Phys. 2020;5:100043.
14. Guck J, et al. The optical stretcher: a novel laser tool to micromanipulate cells. Biophys J. 2001;81(2):767–84.
15. Lim HG, Shung KK. Quantification of inter-erythrocyte forces with ultra-high frequency (410 MHz) single beam acoustic tweezer. Ann Biomed Eng. 2017;45(9):2174–83.
16. Bernecker C, et al. Biomechanics of ex vivo-generated red blood cells investigated by optical tweezers and digital holographic microscopy. Cells. 2021. https://doi.org/10.3390/cells10030552.

17. Keyvan J, Inkyu M. Quantitative investigation of red blood cell three-dimensional geometric and chemical changes in the storage lesion using digital holographic microscopy. J Biomed Opt. 2015;20(11):111218.
18. Gallagher PG. Disorders of erythrocyte hydration. Blood. 2017;130(25):2699–708.
19. Ataullakhanov F, et al. How erythrocyte volume is regulated, or what mathematical models can and cannot do for biology. Biochem Moscow Suppl Ser A. 2009;3:101–15.
20. Jankovsky N, et al. Recent advances in the pathophysiology of PIEZO1-related hereditary xerocytosis. Am J Hematol. 2021;96(8):1017–26.
21. Coste B, et al. Piezo1 and Piezo2 are essential components of distinct mechanically activated cation channels. Science. 2010;330(6000):55–60.
22. Liang X, Howard J. Structural biology: piezo senses tension through curvature. Curr Biol. 2018;28(8):R357–9.
23. Haselwandter CA, MacKinnon R. Piezo's membrane footprint and its contribution to mechanosensitivity. eLife. 2018;7:e41968.
24. Cox CD, et al. Removal of the mechanoprotective influence of the cytoskeleton reveals PIEZO1 is gated by bilayer tension. Nat Commun. 2016;7(1):10366.
25. Syeda R, et al. Piezo1 channels are inherently mechanosensitive. Cell Rep. 2016;17(7):1739–46.
26. Svetina S, Švelc Kebe T, Božič B. A model of piezo1-based regulation of red blood cell volume. Biophys J. 2019;116(1):151–64.
27. Belkacemi A, et al. The TRPV2 channel mediates Ca2+ influx and the Δ9-THC-dependent decrease in osmotic fragility in red blood cells. Haematologica. 2021;106(8):2246–50.
28. Egée S, Kaestner L. The Transient receptor potential vanilloid type 2 (TRPV2) channel-a new druggable Ca(2+) pathway in red cells, implications for red cell ion homeostasis. Front Physiol. 2021;12:677573–677573.
29. Nikolaev YA, et al. Mammalian TRP ion channels are insensitive to membrane stretch. J Cell Sci. 2019;132(23):238360.
30. Guo Y, et al. The Ca(2+)-activated cation channel TRPM4 is a positive regulator of pressure overload-induced cardiac hypertrophy. eLife. 2021;10:e66582.
31. Swain SM, Liddle RA. Piezo1 acts upstream of TRPV4 to induce pathological changes in endothelial cells due to shear stress. J Biol Chem. 2021;296:100171–100171.
32. Swain SM, et al. TRPV4 channel opening mediates pressure-induced pancreatitis initiated by piezo1 activation. J Clin Investig. 2020;130(5):2527–41.
33. Dyrda A, et al. Local membrane deformations activate Ca2+-dependent K+ and anionic currents in intact human red blood cells. PLoS ONE. 2010;5(2):e9447–e9447.
34. Falleroni F, et al. Mechanotransduction in hippocampal neurons operates under localized low picoNewton forces. iScience. 2022;25(2):103807–103807.
35. Falleroni F, Torre V, Cojoc D. Cell mechanotransduction with piconewton forces applied by optical tweezers. Front Cell Neurosci. 2018;12:130–130.
36. Wang H, et al. Fluorescence-coupled micropipette aspiration assay to examine calcium mobilization caused by red blood cell mechanosensing. Eur Biophys J. 2022;51(2):135–46.
37. Ju L, et al. Microscale geometrical modulation of PIEZO1 mediated cell mechanosensing via cytoskeletal redistribution buckle. Res Sq. 2023;13:3093.
38. Hochmuth RM. Micropipette aspiration of living cells. J Biomech. 2000;33(1):15–22.
39. Howard J. Mechanics of motor proteins and the cytoskeleton. Sunderland: Sinauer Associates Publishers; 2001.
40. Kim H-Y. Statistical notes for clinical researchers: nonparametric statistical methods: 1. Nonparametric methods for comparing two groups. Restor Dent Endod. 2014;39(3):235–9.
41. Burns JM, et al. Deterioration of red blood cell mechanical properties is reduced in anaerobic storage. Blood Transfus. 2016;14(1):80–8.
42. Xu Z, et al. Stiffness increase of red blood cells during storage. Microsyst Nanoeng. 2018;4(1):17103.
43. Ma S, et al. Multiscale computational framework for predicting viscoelasticity of red blood cells in aging and mechanical fatigue. Comput Methods Appl Mech Eng. 2022;391:114535.
44. Qiang Y, et al. Mechanical fatigue of human red blood cells. Proc Natl Acad Sci. 2019;116(40):19828–34.
45. Lecklin T, Egginton S, Nash GB. Effect of temperature on the resistance of individual red blood cells to flow through capillary-sized apertures. Pflugers Arch. 1996;432(5):753–9.
46. Smith AS, et al. Myosin IIA interacts with the spectrin-actin membrane skeleton to control red blood cell membrane curvature and deformability. Proc Natl Acad Sci. 2018;115(19):E4377–85.
47. Garcia-Herreros A, et al. Cyclic mechanical stresses alter erythrocyte membrane composition and microstructure and trigger macrophage phagocytosis. Adv Sci. 2022;9(20):2201481.
48. Biswas A, et al. Cholesterol depletion by MβCD enhances cell membrane tension and its variations-reducing integrity. Biophys J. 2019;116(8):1456–68.
49. Ridone P, et al. Disruption of membrane cholesterol organization impairs the activity of PIEZO1 channel clusters. J Gen Physiol. 2020;152(8):e201912515.